Supplemental information for

Reactive Chlorine in the Polluted Marine Boundary Layer during the Halifax Fog and Air Quality Study (HaliFAQS)

Teles C. Furlani[1,a], Emma M. McLay[1], Alex Moravek[1, b], Cameron E. N. Power[2,3], Aldona Wiacek[2,3], Rachel Y.-W. Chang[4], Trevor C. VandenBoer[1], and Cora J. Young[1]

[1] Department of Chemistry, York University, Toronto, Canada

[2] Department of Environmental Science, Saint Mary's University, Halifax, Canada

[3] Department of Astronomy and Physics, Saint Mary's University, Halifax, Canada

[4] Department of Physics and Atmospheric Science, Dalhousie University, Halifax, Canada

[a] Now at Ministry of Environment, Conservation, and Parks, Toronto, Canada

[b] Now at German Environment Agency, Department of Air Quality, Dessau-Rosslau, Germany

S1. Clear sky irradiance calculation

Clear sky solar irradiance was calculated in kW m^{-2} by;[1]

$$I_D = 1.353 \times 1.1 \times \left[(1 - \alpha h)0.7^{AM^{0.678}} + \alpha h\right] \quad \text{SE1}$$

Where, the solar intensity (I_D) arrives on a plane perpendicular to the sun's rays in units of kW/m^2, AM is the air mass zenith, the value of 1.353 kW m^{-2} is the solar constant, the value of 0.7 represents the 70% transmission of radiation to the Earth relative to that incident on the atmosphere, the value of 1.1 is the 10% diffusion component through the atmosphere, the value 0.678 is an empirical fit to the observed data and considers the non-uniformities in the atmospheric layers, α has a value of 0.14, and the location height above sea level (h) has units of kilometers.

The AM term is a function of latitude and calculated by:[2]

$$AM = \frac{1}{cos\theta} \quad \text{SE2}$$

Where θ is the vertical solar zenith angle and calculated by:

$$\cos\theta = \sin\delta\sin\varphi + \cos\delta\cos\varphi\cos\omega \quad \text{SE3}$$

Where δ is declination of the sun, φ is the latitude (defined as positive in the northern hemisphere), and ω is the hour angle. The solar declination is a function of the day of the year and calculated by:[3]

$$\delta = -23.45° \times cos\left(\frac{360}{365} \times (d + 10)\right) \quad \text{SE4}$$

Where d is the day of the year on the Gregorian calendar and ω is a measure of the local time determined by:[3]

$$\omega = 15^\circ\left((LT + \frac{4(\text{Longitude} - 15^0\Delta T_{UTC}) + 9.87sin\left(2(\frac{360}{365}(d-81))\right) - 7.53\cos\left(\frac{360}{365}(d-81)\right) - 1.5\si}{60}) - 12\right) \quad \text{SE5}$$

Where LT is local time and ΔT_{UTC} is the time difference in hours (UTC).

S2. Observations at HaliFAQS ground site

Outdoor air was pulled through a URG PFA-coated aluminum cyclone (URG Corporation, Chapel Hill, North Carolina, USA) with a 2.5 μm aerodynamic diameter cut-off for particulate matter to prevent intrusion and line deposition of local coarse sea spray aerosol. The CRDS sampled ambient air at a flow of 2.0 L min^{-1} from the main inlet line, which resulted in a residence time of 0.75 s for the gas sample. The CRDS sample flow passed through a polytetrafluoroethylene (PTFE) filter (2 μm pore size, 47 mm diameter, TISCH Scientific, North Bend, Ohio, USA) and then two high efficiency particulate air (HEPA) filters contained within the CRDS outer cavity metal compartment, which is heat-regulated to 45 °C. Instances of flagged instrument errors in the CRDS data during ambient observations were removed as this is standard practice in quality control procedures described previously.[4] Supporting NO, NO_x, and O_3 analyzers pulled a total combined flow of 1.6 L min^{-1} from the main inlet. To maintain a total inlet flow of 16.7 L min^{-1}, a mass flow controller (GM50A, MKS instruments, Andover, Massachusetts, USA) maintained an additional 13.1 L min^{-1} of sampling flow using a diaphragm pump.

The OP-FTIR measurement of HCHO used an active broadband mid-IR source modulated by a low-resolution (0.5 cm^{-1}) Fourier transform spectrometer arranged in a monostatic configuration (optical path of 447 m during HaliFAQS). Collimated radiation was focused on a mercury-cadmium-telluride broadband IR detector (spectral response range of 700 -6000 cm^{-1}), where each recorded spectrum is the Fourier transform of a 4-minute average of 960 interferograms collected at 4 Hz. Species concentrations are retrieved from spectra using a non-linear least squares fitting technique accounting for spectral signatures of HCHO and interfering species (H_2O,

N_2O and CH_4) in a smaller spectral window (2745-2800 cm^{-1}), along with instrumental parameters and the background continuum, as described in Wiacek et al.[5]

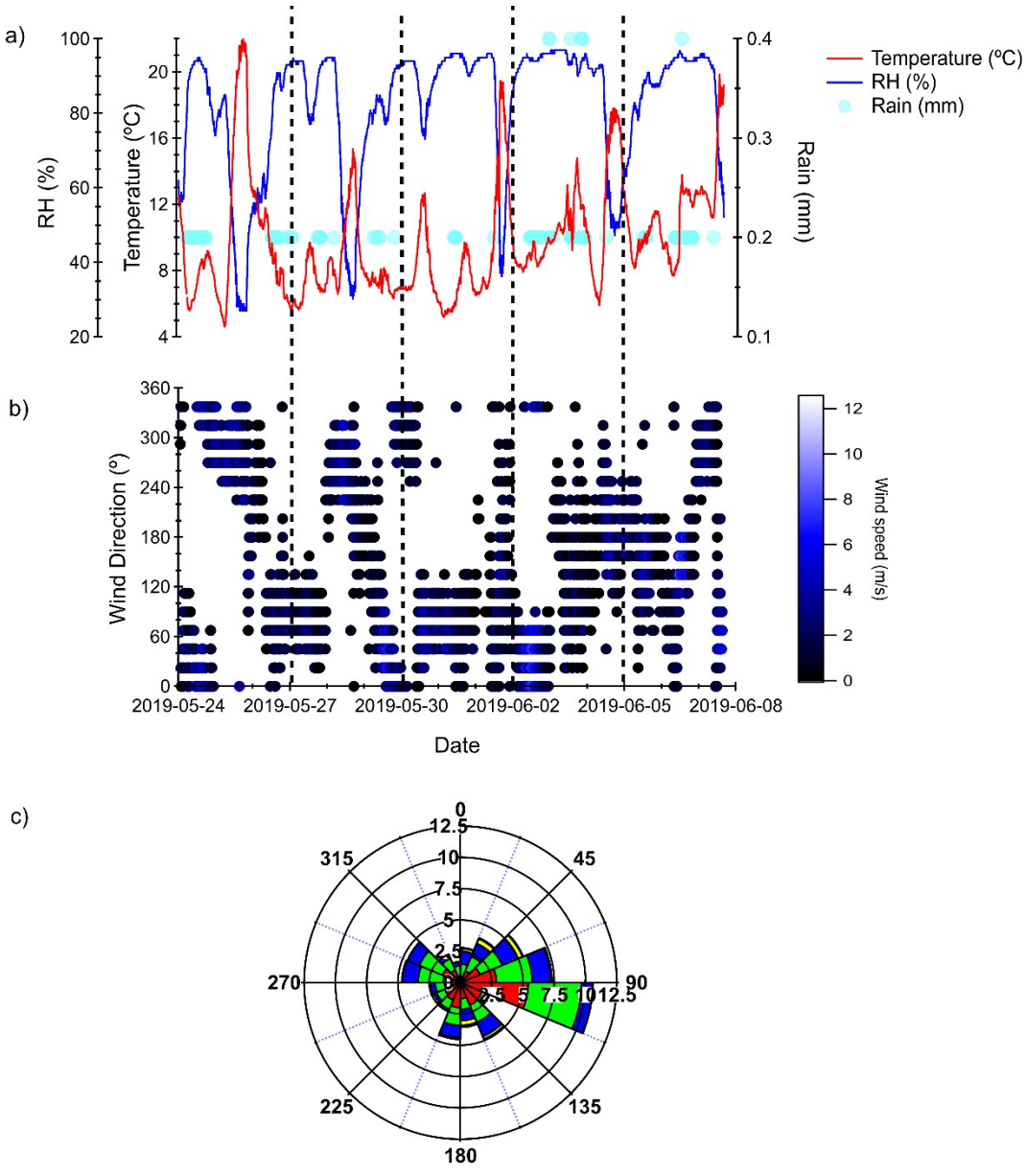

Figure S1. Meteorological data from the campaign including a) temperature (°C), RH (%), rainfall, b) windspeed (m/s) and wind direction (°) and c) a wind rose showing the climatology of the observation period (direction values around circumference; speeds and probability denoted by values extending from centre). Note that meteorological data was only available up to June 8.

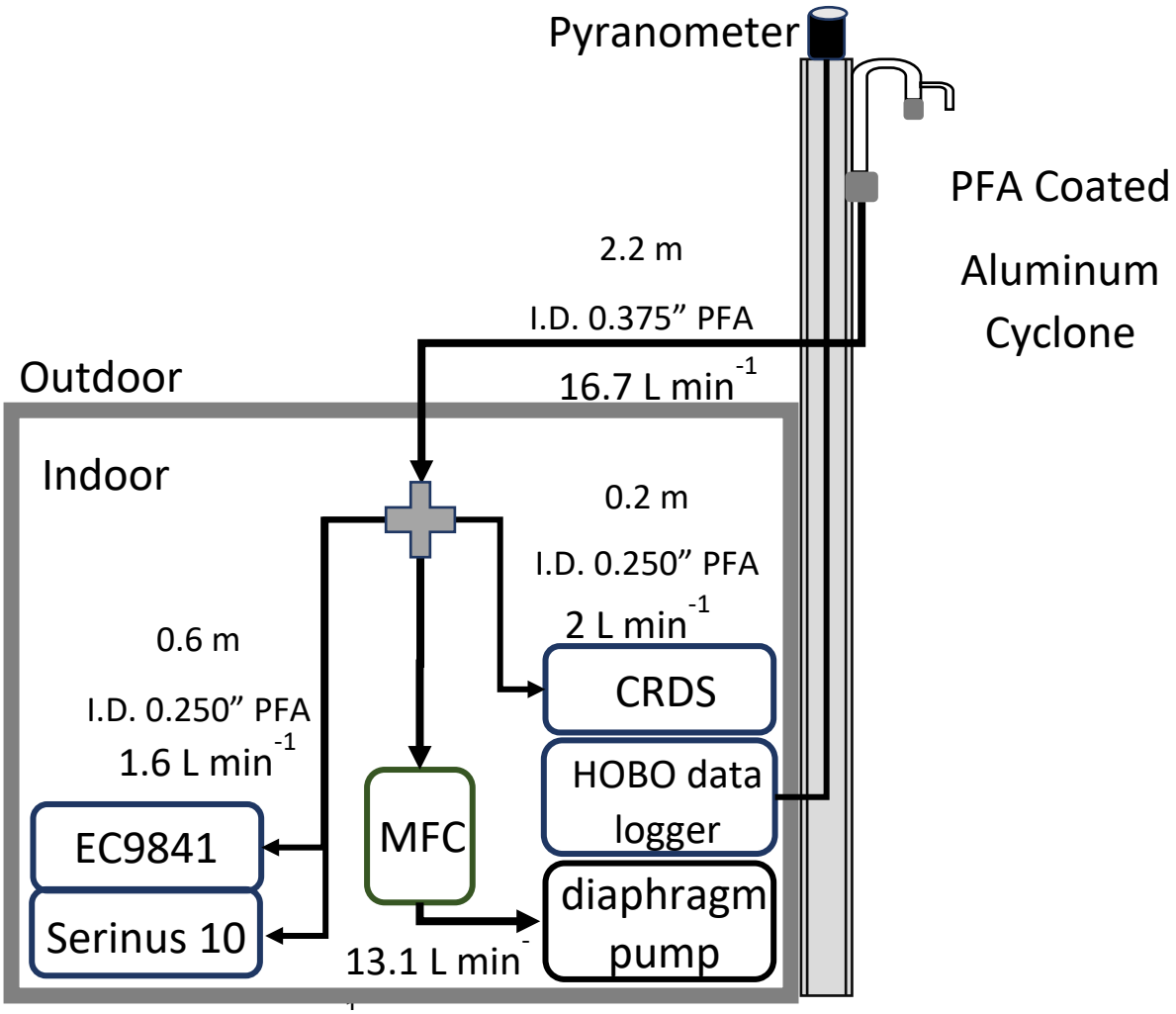

Figure S2. Sampling schematic for all gas analyzers, including flow requirements (black lines with arrows; L min^{-1}), and gas handling tubing lengths in meters, with inner diameters (ID) in inches. The colocation of the pyranometer on top of a rigid mounting post is depicted with a solid black line denoting the communication cable.

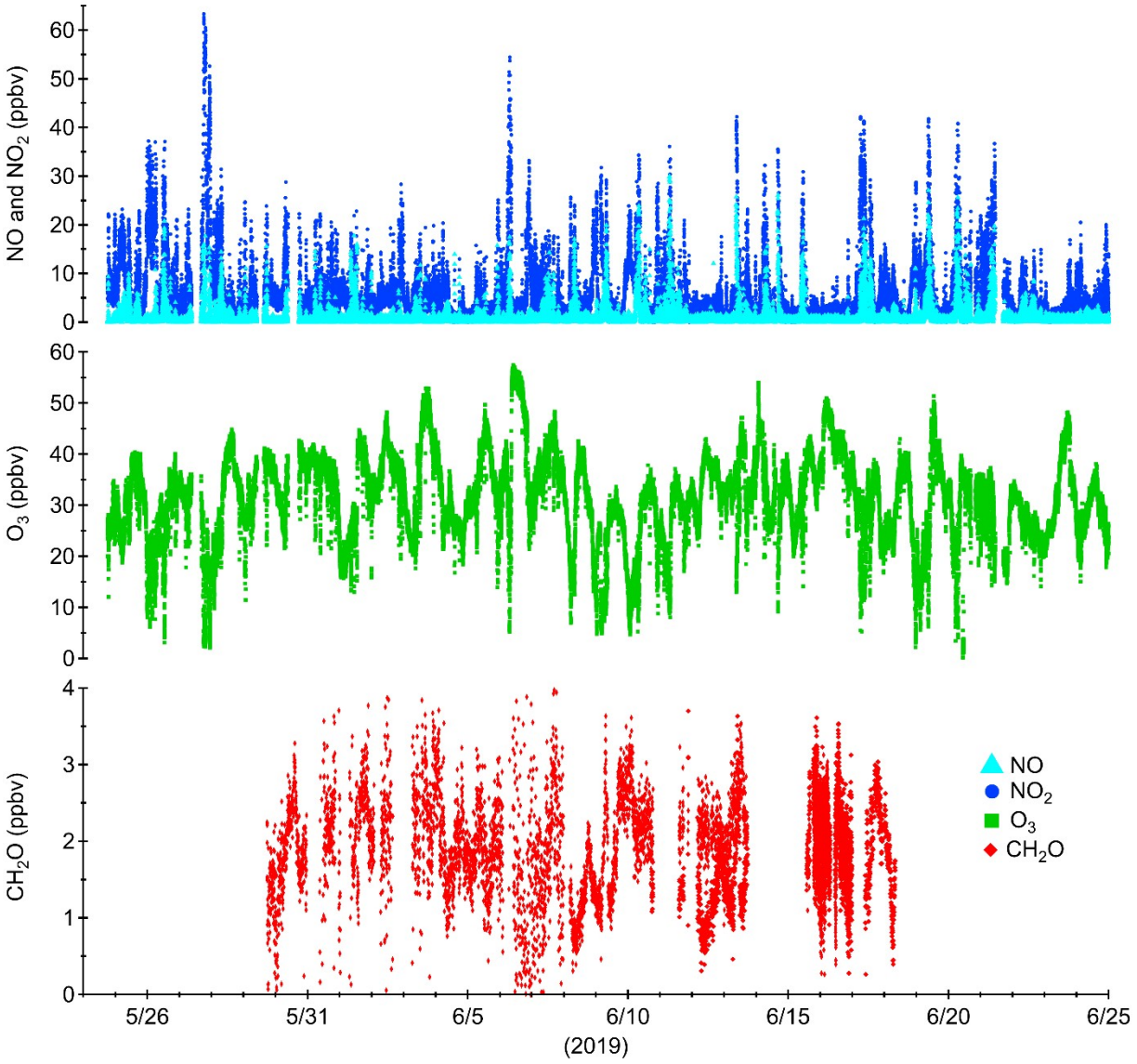

Figure S3. Measurements of NO, NO_2, O_3, and CH_2O during the HaliFAQS campaign. Note that CH_2O data was only possible to obtain for some periods of the campaign.

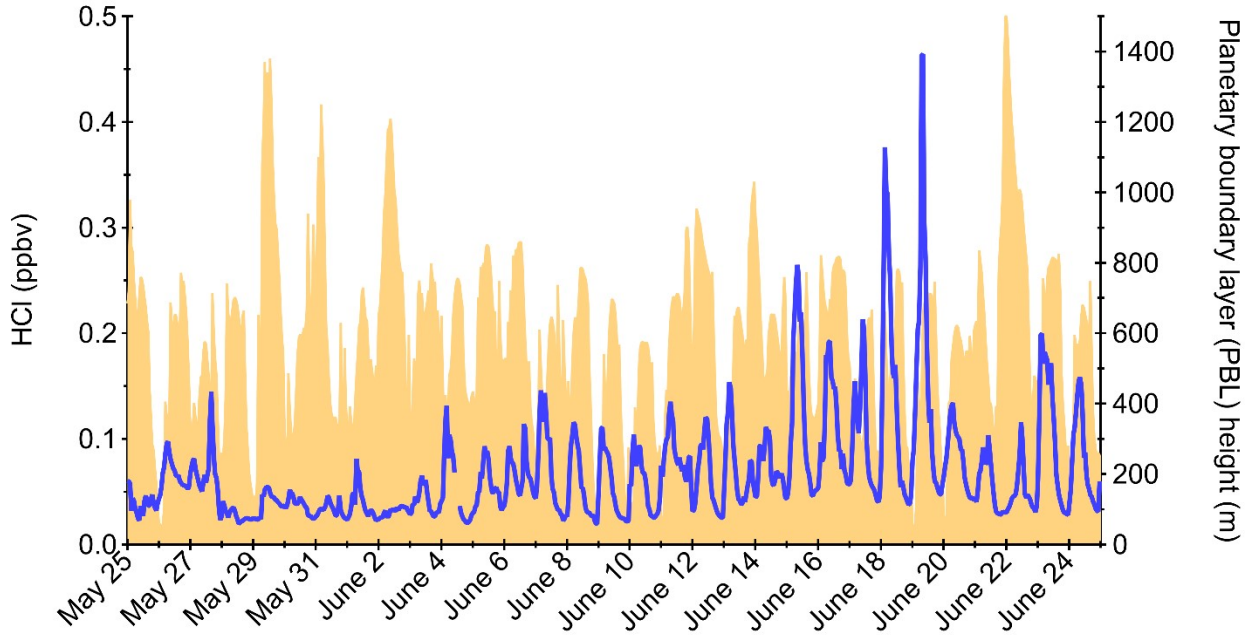

Figure S4. Measured HCl mixing ratio (blue) timeseries and extracted planetary boundary layer (PBL) height (orange) from GEM for the HaliFAQS campaign.

S3. Sensitivity analysis for predicting $ClNO_2$ present at sunrise and modeling subsequent HCl production

Two values of $[ClNO_2]_i$ were calculated, corresponding to high and low HCl deposition conditions to generate upper and lower boundaries due to uncertainties in this term.[6,7] Each calculated $[ClNO_2]_i$ value has an associated uncertainty related to the standard deviation of the fit. These uncertainties for the 8-10:30 window, when converted to relative percentages, were below 16% for all but one day (June 3, a control day) which had the poorest fit with uncertainties of 30% and 27% for 1 cm/s and 6 cm/s deposition velocities, respectively. Table S1 summarizes the $[ClNO_2]_i$ ranges for each modelled date. The effect of choosing timepoints from different time periods other than 08:00 – 10:30 ADT to determine $[ClNO_2]_i$ through the use of the above fitting function is summarized in Table S2. Briefly, the average uncertainties for each time period across the eight days, as can be seen in the final column of Table S2, were lowest for the 8:30 – 10:30 ADT period, indicating that the strongest fits were achieved using this time period. Therefore, 08:00-10:30 ADT was chosen as the period of timepoints to be used for $[ClNO_2]_i$ calculations for all days.

Table S1. List of modelled dates for HCl accumulation, starting with their predicted initial $ClNO_2$ mixing ratios ($[ClNO_2]_i$) from the best fit time period of 8:00-10:30 from the sensitivity analysis, where higher and lower deposition velocity limits for HCl determining the high and low ends of the $ClNO_2$ range, respectively.

Date	Mixing ratio range (pptv)
June 3	12 - 13
June 5	68 - 76
June 7	105 - 118
June 13	149 - 164
June 15	71 - 75
June 17	166 - 187
June 18	427 - 468
June 19	171 - 188

Table S2. Values of $[ClNO_2]_i$ calculated as mixing ratios (ppbv) using the least-squares regression analysis with independent variables ΔHCl, $jClNO_2$, and ΣHCl for the four study days and four control days through a sensitivity analysis of the observational timeframe. The values for both the high and low deposition velocities (dep. vel.) are also determined and assessed for each study day. The uncertainties associated with each value are the standard deviation from the linear fit of the observational data. The average relative uncertainty across all days, as a percentage, for each time period and each deposition velocity case illustrate the strength of the fit period and associated confidence in the $[ClNO_2]_i$ values for all time periods.

Time	Dep. Vel. (cm/s)	Study Date (2019)								Relative Uncertainty (%)
		June 3	June 5	June 7	June 13	June 15	June 17	June 18	June 19	
4:30 – 6:30	1	0.0007 ± 0.0002	0.72 ± 0.39	0.01 ± 0.05	0.24 ± 0.06	0.06 ± 0.01	3.0 ± 2.7	0.35 ± 0.06	0.41 ± 0.26	131
	6	0.0013 ± 0.0002	0.74 ± 0.36	0 ± 0	0.26 ± 0.10	0.04 ± 0.01	3.7 ± 2.6	0.44 ± 0.09	0.80 ± 0.28	34
6:30 – 8:30	1	0.0016 ± 0.0005	0.11 ± 0.04	0.06 ± 0.01	0.15 ± 0.03	0.03 ± 0.01	0.13 ± 0.05	0.35 ± 0.02	0.18 ± 0.05	24
	6	0.0024 ± 0.0004	0.12 ± 0.04	0.07 ± 0.01	0.16 ± 0.04	0.04 ± 0.01	0.14 ± 0.05	0.37 ± 0.03	0.21 ± 0.06	24
8:30 – 10:30	1	0.013 ± 0.002	0.06 ± 0.02	0.11 ± 0.01	0.15 ± 0.01	0.07 ± 0.01	0.17 ± 0.02	0.43 ± 0.04	0.17 ± 0.02	13
	6	0.014 ± 0.002	0.07 ± 0.02	0.12 ± 0.01	0.17 ± 0.01	0.08 ± 0.01	0.19 ± 0.02	0.47 ± 0.04	0.19 ± 0.02	12
5:30 – 8:00	1	0.0010 ± 0.0001	0.08 ± 0.07	0.05 ± 0.01	0.19 ± 0.04	0.05 ± 0.02	0.19 ± 0.07	0.36 ± 0.02	0.28 ± 0.05	30
	6	0.0019 ± 0.0001	0.09 ± 0.07	0.06 ± 0.01	0.18 ± 0.05	0.05 ± 0.02	0.22 ± 0.08	0.37 ± 0.04	0.32 ± 0.06	30
8:00 – 10:30	1	0.012 ± 0.0018	0.068 ± 0.021	0.11 ± 0.011	0.15 ± 0.0090	0.071 ± 0.0076	0.17 ± 0.015	0.43 ± 0.033	0.17 ± 0.018	12
	6	0.012 ± 0.0019	0.076 ± 0.021	0.12 ± 0.011	0.16 ± 0.011	0.075 ± 0.0079	0.19 ± 0.018	0.47 ± 0.034	0.19 ± 0.019	12

S4. Yield of HCl from reactions of Cl

Radical reactivity determinations are rare for Cl, so several assumptions are required in assessing the fraction of Cl that forms HCl. In this case, we have used a lower limit of 77 %. This accounts for non-HCl forming Cl losses through reaction with O_3 (up to 8.8 %), alkenes (up to 7.0 %), and aromatics (7.6 %), for a total of 23 %. We have also considered an upper limit of 100 %. The rationale for this is discussed below, considering reactions with inorganic and organic molecules.

Inorganic

Reactions of Cl with abundant inorganic gases (i.e., NO, NO_2, O_3) lead to non-HCl products. In the case of NO and NO_2, these are short-lived photolabile Cl_y:

$Cl + NO \rightarrow ClNO$ (SR-1)

$Cl + NO_2 \rightarrow ClNO_2$ (SR-2)

Because these ultimately act as short-lived reservoirs for Cl, we have not considered them as consequential in the overall fate of Cl and therefore the yield of HCl. Reaction of Cl with O_3 is more complex. The reaction of Cl with O_3 leads to ClO:

$Cl + O_3 \rightarrow ClO$ (SR-3)

The major fate of ClO is reaction with NO and NO_2.[8]

$ClO + NO \rightarrow Cl + NO_2$ (SR-4)

$ClO + NO_2 \rightarrow ClONO_2$ (SR-5)

While reaction with NO leads to regeneration of Cl, reaction with NO_2 leads to formation of chlorine nitrate ($ClONO_2$).

We can calculate the reactivity of ClO using our measurements of NO:

$Reactivity_{Cl+NO} = k_{Cl+NO}[NO]$

Using a similar calculation for NO_2, we can determine the fraction of ClO that forms $ClONO_2$. Between 6 am and noon, the fraction of ClO that reacts via SR-5 to form $ClONO_2$ is 94 to 98 %. The fate of $ClONO_2$ is photolysis to re-form Cl or ClO or deposition.

$ClONO_2 + h\nu \rightarrow Cl + NO_3$ (SR-6)

$ClONO_2 + h\nu \rightarrow ClO + NO_2$ (SR-7)

There is uncertainty in the rate and therefore extent of deposition of $ClONO_2$. A recent modelling study by Edwards and Young[8] showed that ~2/3 of $ClONO_2$ regenerated Cl directly by photolysis (via R-S6), with 20-25 % deposited, and the remainder photolyzing to form ClO (SR-7).

Because of the rarity of Cl reactivity assessments, we have used for reference a reactivity assessment for a North American coastal city (Los Angeles, CA) in late spring.[9] We assume that this represents a reasonable proxy for Halifax. In the Los Angeles-based assessment, the fraction of total Cl reactivity for O_3 in the morning (between 6 am and noon) ranged from 3.9 to 8.8 %. If that same reactivity fraction translated to Halifax during our study, that would lead to a maximum of 2.1 % of Cl reactions leading to non-HCl fate through loss to deposition via $ClONO_2$. However, given the significant uncertainties in this estimation, we decided to consider a larger range of possibilities to present a broader assessment of the fate of Cl: that reactions with O_3 do not lead to any non-HCl forming Cl loss and that all reactions with O_3 lead to non-HCl forming Cl loss (Table S3). This highlights the substantial uncertainties that persist in our knowledge of these pathways, which could be the subject of future atmospheric chemistry research intensives in regions with substantial photolabile Cl_y.

Organic

For H-abstraction reactions between organics and Cl, the product will be HCl. However, it is also possible for Cl to add to unsaturated molecules. In the case of Cl addition, the product will be a Cl-containing radical. The ratio of addition to abstraction is not well characterized for many unsaturated atmospheric organics. For isoprene, the fraction that reacts by H-abstraction is 0.15.[10] In the case of aromatics, Cl reacts exclusively with H-containing substituents (if they exist) rather than addition to the aromatic ring. In the Los Angeles Cl reactivity assessment,[9] loss due to reaction with alkenes (i.e., biogenics and non-biogenic alkenes) was 5.0 to 7.0 % of total Cl reactivity between 6 am and noon. During the same period, loss due to reaction with aromatics was 7.6 to 8.9 % of total Cl reactivity. We assume that 0 to 20 % of alkene reactions lead to HCl formation and 85 to 100 % of aromatic reactions lead to HCl formation (Table S3). Thus, the maximum non-HCl forming Cl loss contributed by reactions with alkenes and aromatics are 7.0 and 7.6 %, respectively.

Table S3. Assessment of maximum non-HCl forming Cl losses from springtime Los Angeles Cl reactivity. This was used to generate the lower limit of HCl formation from Cl reactions (i.e., 77 %).

	Fraction of reactivity from Los Angeles between 6 am and noon		Fraction leading to non-HCl losses		Maximum non-HCl forming losses
Reactant	Min	Max	Min	Max	
O3	0.039	0.088	0	1	0.088
Alkenes	0.050	0.070	0.2	1	0.070
Aromatics	0.076	0.089	0	0.85	0.076
				Total	**0.23**

S5. Measurements and sources of gaseous hydrochloric acid (HCl)

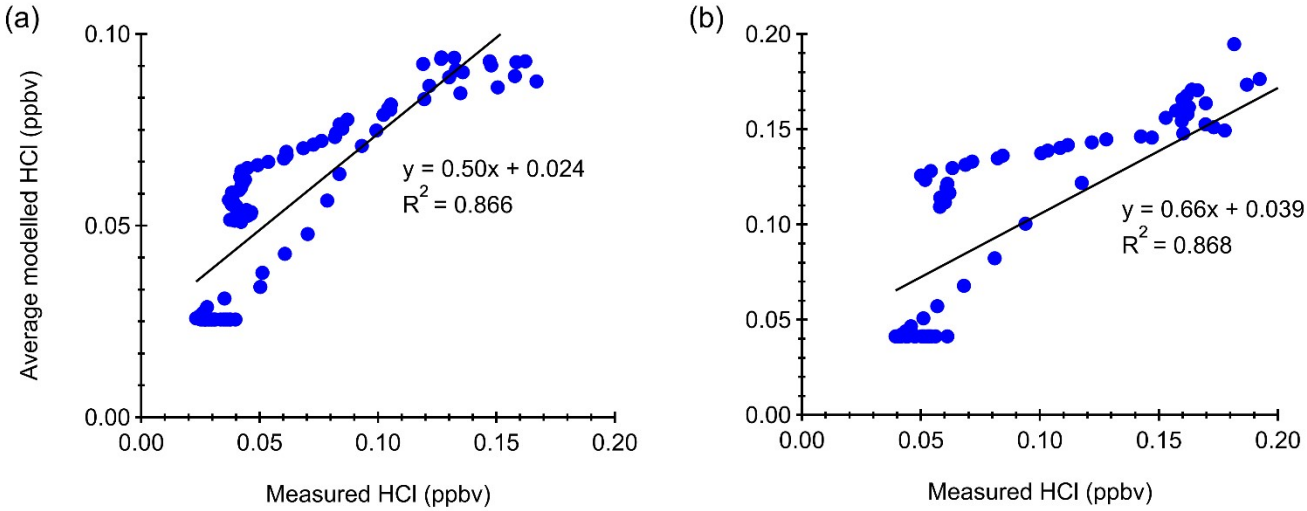

Figure S5. Modelled HCl in ppbv correlation with the measured HCl for a) June 13 and b) June 18, the two days used for modelling radical formation.

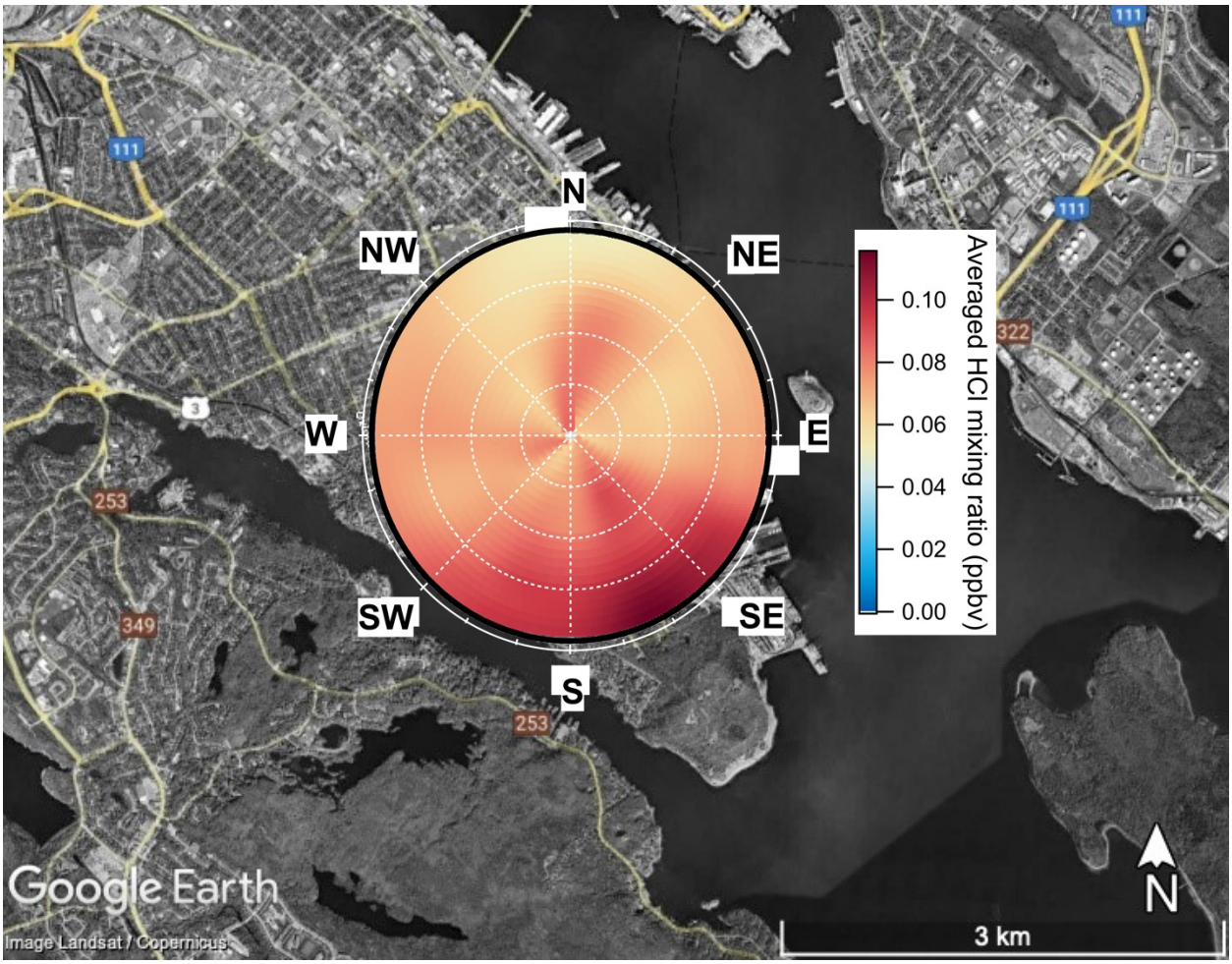

Figure S6. Polar plot of HCl overlayed on a Google Earth image of the campaign location. The radial axis is wind speed from 0–9 m s^{-1}.

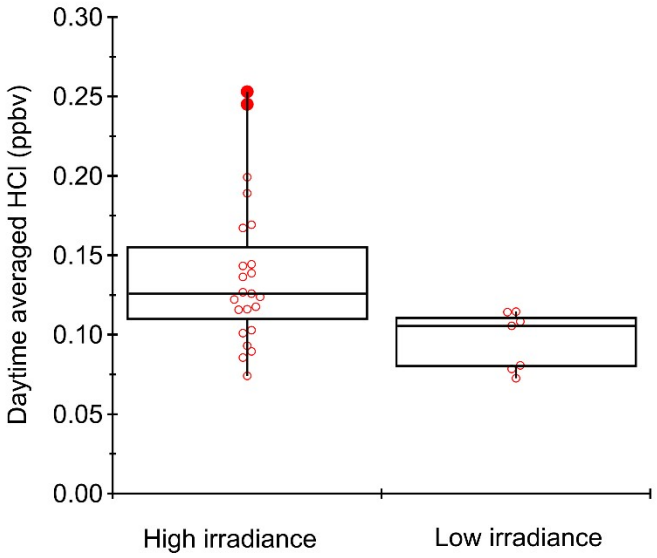

Figure S7. Box (1st and 3rd quartiles) and whisker (maximum range) plot of average daytime HCl mixing ratios for high and low irradiance days. The solid line within each box represents the median, open circles represent individual measurements, and solid circles are outliers from the assumption of a normal distribution. We defined high irradiance days as those within 25% of maximum integrated irradiance day during the campaign and the remaining days were therefore classed as low irradiance.

Table S4. Summary of global HCl measurements reported for the marine boundary layer. Numbers in brackets for HCl mixing ratios are the reported or calculated measurement dataset average.

Location	Date	Method	HCl mixing ratio range (pptv)	Reference
Halifax, Nova Scotia, Canada	May–June 2019	CRDS	55–572 (97)	This study
Central California Coast, US	May–June 2010	Acetate CI-TOFMS	0–2800 (440)	Crisp et al.[11]
Southern California Coast	May–June 2010	Acetate CI-TOFMS	0 to >16000 (2200)	Crisp et al.[11]
Claremont, California, US	September 1985	Denuder/IC	0–2000	Appel et al.[12]
Claremont, California, US	September 1985	Dichotomous sampler	0–1600	John et al.[13]
Glendora, California, US	August 1986	Filter/LC	0–850 (500)	Grosjean.[14]
Southern California, US	1986	Denuder/IC	400–1300	Eldering et al.[15]
Colchester, UK	March–April 1987	Filter/IC	100–1200	Sturges and Harrison.[16]
Colchester, UK	Feb 1987 — Jan 1988	Filter/IC	200–1200 (500)	Harrison and Allen.[17]
Petten, Netherlands	March–August 1987	Denuder/IC	70–3000	Keuken et al.[18]
Umeå, Sweden	January 1990	Diffusion Scrubber/IC	200–1000	Lindgren.[19]
Umeå, Sweden	July 1990	Diffusion Scrubber/IC	100–600	Lindgren.[19]
Umeå, Sweden	September 1990	Diffusion Scrubber/IC	20–300	Lindgren.[19]
Manhattan, New York, US	July 1999— June 2000	Denuder/IC	10–2000 (300)	Bari et al.[20]
Bronx, New York, US	July 1999— June 2000	Denuder/IC	10–1800 (300)	Bari et al.[20]
Sydney, Florida, US	May 2002	Denuder/IC	<10–5600 (700)	Dasgupta et al.[21]
Bermuda	July–September	Filter/IC	200–400	Keene et al.[22]

	1988			
East Coast, US	July–September 1988	Filter/IC	500–1200	Keene et al.[22]
Miami, Florida, US	January 1992	Tandem Mist Chamber/IC	40–270	Pszenny et al.[23]
Tudor Hill, Bermuda	April–May 1996	Tandem Mist Chamber/IC	100–900	Keene and Savoie.[24]
Oahu, Hawaii, US	September 1999	Tandem Mist Chamber/IC	30–300	Pszenny et al.[25]
Dumont d'Urville, Antarctica	Dec 2000—Dec 2001	Tandem Mist Chamber/IC	30–300	Jourdain and Legrand. [26]
S. Carolina, US to Canadian Coast	July–August 2002	Tandem Mist Chamber/IC	<25–4500	Keene et al.[27]
Germany to South Africa	October–November 2003	Tandem Mist Chamber/IC	20–1400	Keene et al.[28]
Appledore Island, Maine, US	July–August 2004	Tandem Mist Chamber/IC	5–5800 (600)	Keene et al.[29]
N. Pacific Ocean near Alaska, US	May 2006	SF_6 CIMS	6–100 (30)	Kim et al.[30]
Sao Vicente Island, Cape Verde	May–June 2007	Tandem Mist Chamber/IC	50–600	Lawler et al.[31]
Cyprus	July–August 2014	Iodide CI-QMS	<135–3000 (790)	Eger et al.[32]
East Coast, US	February–March 2015	Iodide CI-TOFMS	199–380	Haskins et al.[33]
St John's, Newfoundland, Canada	April 2017	CRDS	<20–1210 (63)	Angelucci et al.[34]

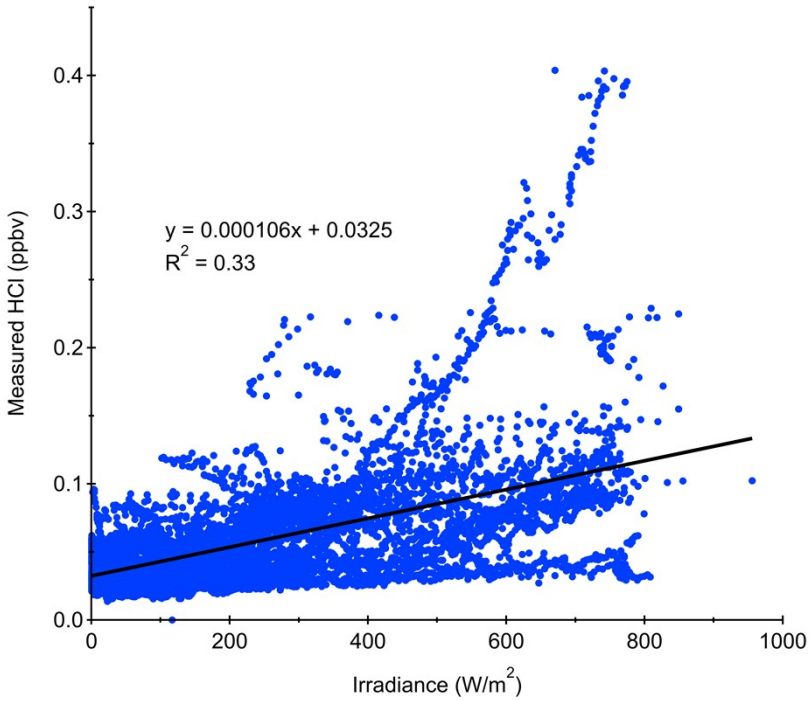

Figure S8. Measured HCl concentration correlation with irradiance for mornings only (5:30-10:30) during the whole HaliFAQS campaign duration.

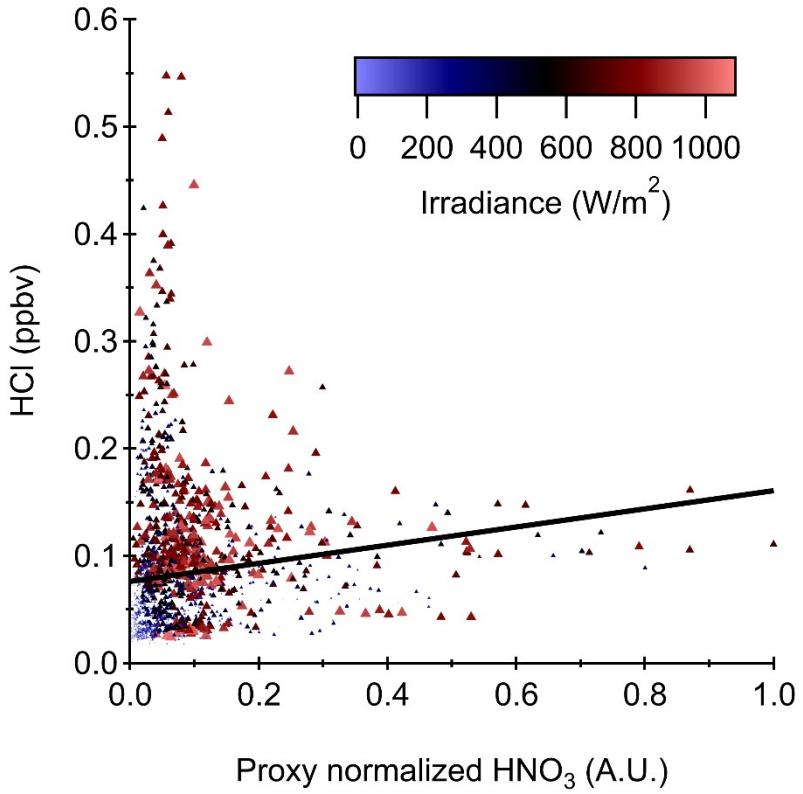

Figure S9. Measured HCl plotted against normalized HNO_3 colored by irradiance for daytime only. Black line is the linear regression best fit line (slope=0.085, R^2=0.018). Proxy HNO_3 is calculated by multiplying the mixing ratio of NO_2 by the irradiance, as an indirect estimate of OH available for reaction with NO_2.

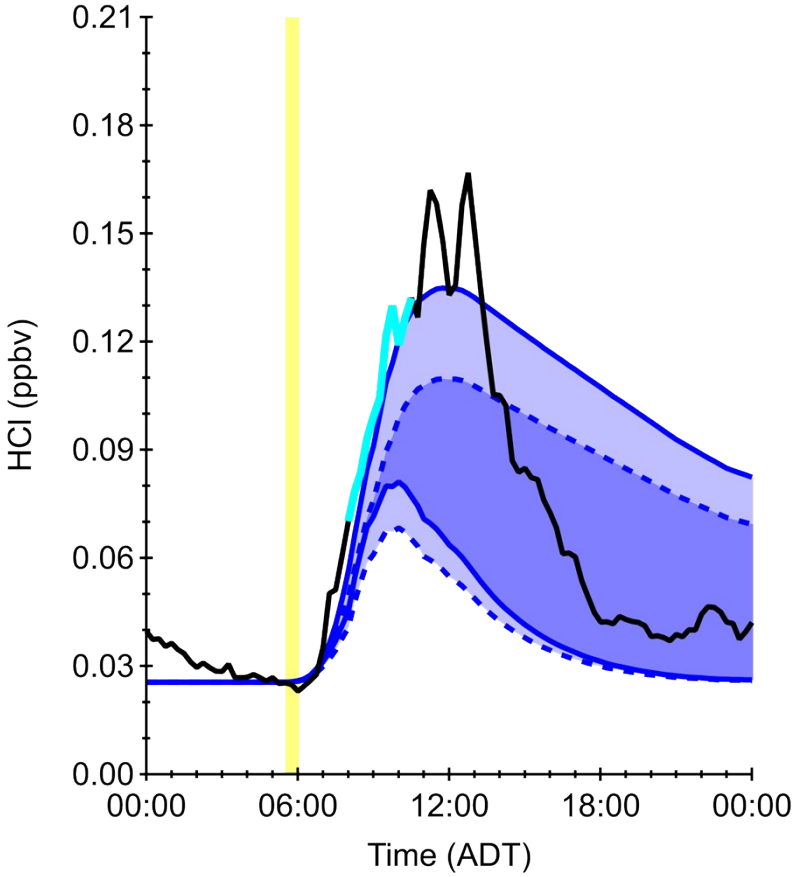

Figure S10. Measured HCl (black) and modelled HCl (blue) predicted from photolysis of the initial $ClNO_2$ estimated for June 13 (category (i) day). Blue shading indicates the uncertainty in the modelled HCl from the range of deposition velocities and conversion efficiencies. From top to bottom, the 4 modelled traces are those for 100% CE and 1 cm s^{-1} deposition velocity, 77% CE and 1 cm s^{-1} deposition velocity, 100% CE and 6 cm s^{-1} deposition velocity, and 77% CE and 6 cm s-1 deposition velocity. and 77% CEs for 1 cm s^{-1} deposition velocity, followed by the same CEs and 6 cm s^{-1}). The yellow vertical line denotes time at sunrise and the cyan section of the measured HCl trace indicates the period used to estimate the amount of initial $ClNO_2$ present in the first part of the box model.

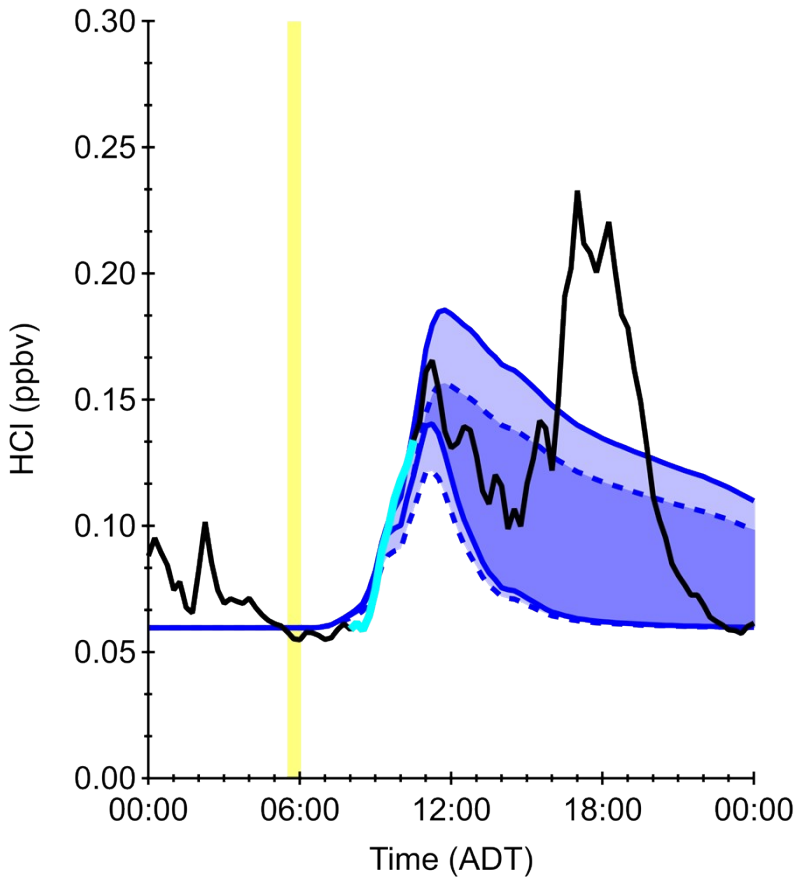

Figure S11. Measured HCl (black) and modelled HCl (blue) predicted from photolysis of the initial $ClNO_2$ estimated for June 17 (category (ii) day). Blue shading indicates the uncertainty in the modelled HCl from the range of deposition velocities and conversion efficiencies. From top to bottom, the 4 modelled traces are those for 100% CE and 1 cm s^{-1} deposition velocity, 77% CE and 1 cm s^{-1} deposition velocity, 100% CE and 6 cm s^{-1} deposition velocity, and 77% CE and 6 cm s-1 deposition velocity. and 77% CEs for 1 cm s^{-1} deposition velocity, followed by the same CEs and 6 cm s^{-1}). Dotted traces represent 77% CE cases while solid lines indicate the 100% CE cases . The yellow vertical line denotes time at sunrise and the cyan section of the measured HCl trace indicates the period used to estimate the amount of initial $ClNO_2$ present in the first part of the box model.

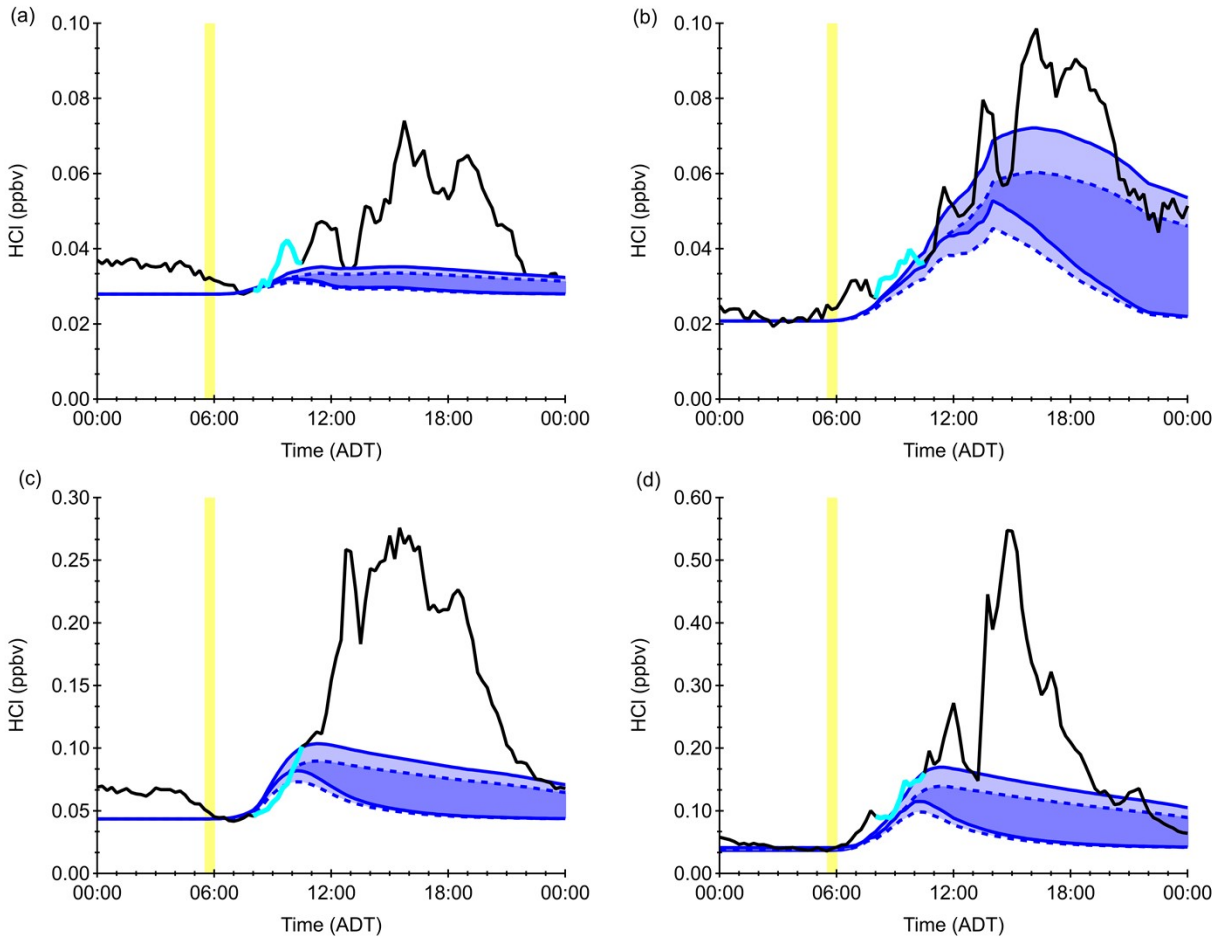

Figure S12. Measured HCl (black) and modelled HCl (blue) predicted from photolysis of the initial $ClNO_2$ estimated for a) June 3, b) June 5, c) June 15, and d) June 19, all category (iii) days. Blue shading indicates the uncertainty in the modelled HCl from the range of deposition velocities and conversion efficiencies. From top to bottom, the 4 modelled traces are those for 100% CE and 1 cm s^{-1} deposition velocity, 77% CE and 1 cm s^{-1} deposition velocity, 100% CE and 6 cm s^{-1} deposition velocity, and 77% CE and 6 cm s-1 deposition velocity. and 77% CEs for 1 cm s^{-1} deposition velocity, followed by the same CEs and 6 cm s^{-1}). The yellow vertical line denotes time at sunrise and the cyan section of the measured HCl trace indicates the period used to estimate the amount of initial $ClNO_2$ present in the first part of the box model. Note that the y-axis scales differ between the panels.

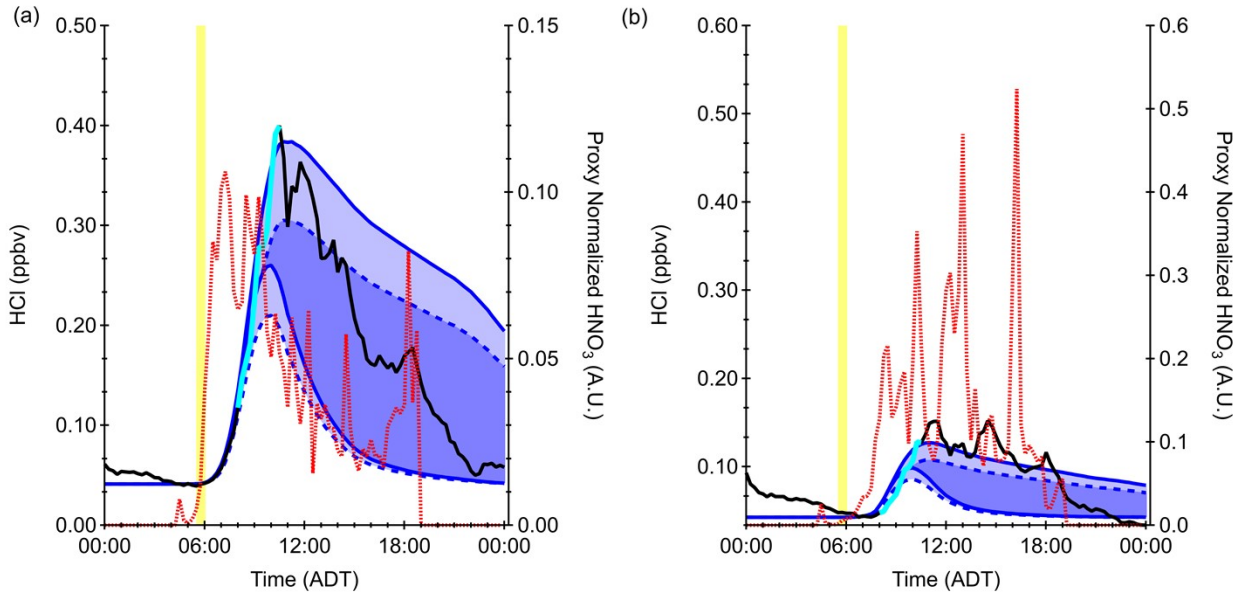

Figure S13. Measured HCl (black), modelled HCl predicted from photolysis of the initial $ClNO_2$ (blue), and proxy normalized HNO_3 (red dotted) for a) June 18 (category (i) day with only a morning mode) and b) June 7 (category (ii) day with bimodal features. Blue shading indicates the uncertainty in the modelled HCl from the range of deposition velocities and conversion efficiencies. From top to bottom, the 4 modelled traces are those for 100% CE and 1 cm s^{-1} deposition velocity, 77% CE and 1 cm s^{-1} deposition velocity, 100% CE and 6 cm s^{-1} deposition velocity, and 77% CE and 6 cm s-1 deposition velocity. and 77% CEs for 1 cm s^{-1} deposition velocity, followed by the same CEs and 6 cm s^{-1}). The yellow vertical line denotes time at sunrise and the cyan section of the measured HCl trace indicates the period used to estimate the amount of initial $ClNO_2$ present in the first part of the box model. Note that the y-axes scales differ between the panels.

References

(1) Meinel, A. B.; Meinel, M. P. Applied Solar Energy Addison. Wesley Publishing Co 1976.

(2) Kasten, F.; Young, A. T. Revised Optical Air Mass Tables and Approximation Formula. *Appl Opt* **1989**, *28* (22), 4735–4738. https://doi.org/10.1364/AO.28.004735.

(3) Woolf, H. On the Computation of Solar Elevation Angles and the Determination of Sunrise and Sunset Times; 1968.

(4) Furlani, T. C.; Veres, P. R.; Dawe, K. E. R.; Neuman, J. A.; Brown, S. S.; VandenBoer, T. C.; Young, C. J. Validation of a New Cavity Ring-down Spectrometer for Measuring Tropospheric Gaseous Hydrogen Chloride. *Atmos. Meas. Tech. Discuss.* **2021**, *2021*, 1–30. https://doi.org/10.5194/amt-2021-105.

(5) Wiacek, A.; Li, L.; Tobin, K.; Mitchell, M. Characterization of Trace Gas Emissions at an Intermediate Port. *Atmos Chem Phys* **2018**, *18* (19), 13787–13812. https://doi.org/10.5194/acp-18-13787-2018.

(6) Place, B. K.; Young, C. J.; Ziegler, S. E.; Edwards, K. A.; Salehpoor, L.; VandenBoer, T. C. Passive Sampling Capabilities for Ultra-Trace Quantitation of Atmospheric Nitric Acid (HNO3) in Remote Environments. *Atmos Environ* **2018**, *191* (October 2018), 360–369. https://doi.org/10.1016/j.atmosenv.2018.08.030.

(7) Crisp, T. A.; Lerner, B. M.; Williams, E. J.; Quinn, P. K.; Bates, T. S.; Bertram, T. H. Observations of Gas Phase Hydrochloric Acid in the Polluted Marine Boundary Layer. *Journal of Geophysical Research*. 2014, pp 6897–6915. https://doi.org/10.1002/2013JD020992.

(8) Crisp, T. a; Lerner, B. M.; Williams, E. J.; Quinn, P. K.; Bates, T. S.; Bertram, T. H. Observations of Gas Phase Hydrochloric Acid in the Polluted Marine Boundary Layer. *Journal of Geophysical Research: Atmospheres* **2014**, 6897–6915. https://doi.org/10.1002/2013JD020992.Received.

(9) Appel, B. R.; Tokiwa, Y.; Povard, V.; Kothny, E. L. The Measurement of Atmospheric Hydrochloric Acid in Southern California. *Atmospheric Environment. Part A. General Topics* **1991**, *25* (2), 525–527. https://doi.org/https://doi.org/10.1016/0960-1686(91)90325-2.

(10) John, W.; Wall, S. M.; Ondo, J. L. A New Method for Nitric Acid and Nitrate Aerosol Measurement Using the Dichotomous Sampler. *Atmospheric Environment (1967)* **1988**, *22* (8), 1627–1635. https://doi.org/https://doi.org/10.1016/0004-6981(88)90390-3.

(11) Grosjean, D. Liquid-Chromatography Analysis of Chloride and Nitrate with “Negative” Ultraviolet Detection: Ambient Levels and Relative Abundance of Gas-Phase Inorganic and Organic Acids in Southern California. *Environmental Science & Technology* **1990**, *24* (1), 77–81. https://doi.org/10.1021/es00071a007.

(12) Eldering, A. M.; Solomon, P. A.; Salmon, L. G.; Fall, T.; Cass, G. R. Hydrochloric Acid: A Regional Perspective on Concentrations and Formation in the Atmosphere of Southern California. *Atmospheric Environment Part A, General Topics* **1991**, *25* (10), 2091–2102. https://doi.org/10.1016/0960-1686(91)90086-M.

(13) Sturges, W. T.; Harrison, R. M. The Use of Nylon Filters to Collect Hcl: Efficiencies, Interferences and Ambient Concentrations. *Atmospheric Environment (1967)* **1989**, *23* (9), 1987–1996. https://doi.org/https://doi.org/10.1016/0004-6981(89)90525-8.

(14) Harrison, R. M.; Allen, A. G. Measurements of Atmospheric HNO3, HCl and Associated Species on a Small Network in Eastern England. *Atmospheric Environment. Part A. General Topics* **1990**, *24* (2), 369–376. https://doi.org/https://doi.org/10.1016/0960-1686(90)90116-5.

(15) Keuken, M. P.; Schoonebeek, C. A. M.; van Wensveen-Louter, A.; Slanina, J. Simultaneous Sampling of NH3, HNO3, HC1, SO2 and H2O2 in Ambient Air by a Wet Annular Denuder System. *Atmospheric Environment (1967)* **1988**, *22* (11), 2541–2548. https://doi.org/https://doi.org/10.1016/0004-6981(88)90486-6.

(16) Lindgren, P. F. Diffusion Scrubber-Ion Chromatography for the Measurement of Trace Levels of Atmospheric HCl. *Atmospheric Environment. Part A. General Topics* **1992**, *26* (1), 43–49. https://doi.org/https://doi.org/10.1016/0960-1686(92)90259-N.

(17) Bari, A.; Ferraro, V.; Wilson, L. R.; Luttinger, D.; Husain, L. Measurements of Gaseous HONO, HNO3, SO2, HCl, NH3, Particulate Sulfate and PM2.5 in New York, NY. *Atmospheric Environment* **2003**, *37* (20), 2825–2835. https://doi.org/10.1016/S1352-2310(03)00199-7.

(18) Dasgupta, P. K.; Campbell, S. W.; Al-Horr, R. S.; Ullah, S. M. R.; Li, J.; Amalfitano, C.; Poor, N. D. Conversion of Sea Salt Aerosol to NaNO3 and the Production of HCl: Analysis of Temporal Behavior of Aerosol Chloride/Nitrate and Gaseous HCl/HNO3 Concentrations with AIM. *Atmospheric Environment* **2007**, *41* (20), 4242–4257. https://doi.org/https://doi.org/10.1016/j.atmosenv.2006.09.054.

(19) Keene, W. C.; Pszenny, A. A. P.; Jacob, D. J.; Duce, R. A.; Galloway, J. N.; Schultz-Tokos, J. J.; Sievering, H.; Boatman, J. F. The Geochemical Cycling of Reactive Chlorine through the Marine Troposphere. *Global Biogeochemical Cycles* **1990**, *4* (4), 407–430. https://doi.org/https://doi.org/10.1029/GB004i004p00407.

(20) Pszenny, A. A. P.; Keene, W. C.; Jacob, D. J.; Fan, S.; Maben, J. R.; Zetwo, M. P.; Springer-Young, M.; Galloway, J. N. Evidence of Inorganic Chlorine Gases Other than Hydrogen Chloride in Marine Surface Air. *Geophysical Research Letters* **1993**, *20* (8), 699–702. https://doi.org/10.1029/93GL00047.

(21) Keene, W. C.; Savoie, D. L. The PH of Deliquesced Sea-Salt Aerosol in Polluted Marine Air. *Geophysical Research Letters* **1998**, *25* (12), 2181–2184. https://doi.org/https://doi.org/10.1029/98GL01591.

(22) Pszenny, A. A. P.; Moldanová, J.; Keene, W. C.; Sander, R.; Maben, J. R.; Martinez, M.; Crutzen, P. J.; Perner, D.; Prinn, R. G. Halogen Cycling and Aerosol PH in the Hawaiian Marine Boundary Layer. *Atmos. Chem. Phys.* **2004**, *4* (1), 147–168. https://doi.org/10.5194/acp-4-147-2004.

(23) Jourdain, B.; Legrand, M. Year-Round Records of Bulk and Size-Segregated Aerosol Composition and HCl and HNO3 Levels in the Dumont d'Urville (Coastal Antarctica) Atmosphere: Implications for Sea-Salt Aerosol Fractionation in the Winter and Summer. *Journal of Geophysical Research:*

Atmospheres **2002**, *107* (D22), ACH 20-1-ACH 20-13. https://doi.org/https://doi.org/10.1029/2002JD002471.

(24) Keene, W. C.; Pszenny, A. A. P.; Maben, J. R.; Stevenson, E.; Wall, A. Closure Evaluation of Size-Resolved Aerosol PH in the New England Coastal Atmosphere during Summer. *Journal of Geophysical Research: Atmospheres* **2004**, *109* (D23). https://doi.org/https://doi.org/10.1029/2004JD004801.

(25) Keene, W. C.; Long, M. S.; Pszenny, A. A. P.; Sander, R.; Maben, J. R.; Wall, A. J.; O'Halloran, T. L.; Kerkweg, A.; Fischer, E. V; Schrems, O. Latitudinal Variation in the Multiphase Chemical Processing of Inorganic Halogens and Related Species over the Eastern North and South Atlantic Oceans. *Atmos Chem Phys* **2009**, *9* (19), 7361–7385. https://doi.org/10.5194/acp-9-7361-2009.

(26) Keene, W. C.; Stutz, J.; Pszenny, A. A. P.; Maben, J. R.; Fischer, E. V; Smith, A. M.; von Glasow, R.; Pechtl, S.; Sive, B. C.; Varner, R. K. Inorganic Chlorine and Bromine in Coastal New England Air during Summer. *Journal of Geophysical Research: Atmospheres* **2007**, *112* (D10). https://doi.org/10.1029/2006JD007689.

(27) Kim, S.; Huey, L. G.; Stickel, R. E.; Pierce, R. B.; Chen, G.; Avery, M. A.; Dibb, J. E.; Diskin, G. S.; Sachse, G. W.; McNaughton, C. S.; Clarke, A. D.; Anderson, B. E.; Blake, D. R. Airborne Measurements of HCl from the Marine Boundary Layer to the Lower Stratosphere over the North Pacific Ocean during INTEX-B. *Atmos. Chem. Phys. Discuss.* **2008**, *2008*, 3563–3595. https://doi.org/10.5194/acpd-8-3563-2008.

(28) Lawler, M. J.; Finley, B. D.; Keene, W. C.; Pszenny, A. A. P.; Read, K. A.; von Glasow, R.; Saltzman, E. S. Pollution-Enhanced Reactive Chlorine Chemistry in the Eastern Tropical Atlantic Boundary Layer. *Geophys Res Lett* **2009**, *36* (8). https://doi.org/10.1029/2008GL036666.

(29) Eger, P. G.; Helleis, F.; Schuster, G.; Phillips, G. J.; Lelieveld, J.; Crowley, J. N. Chemical Ionization Quadrupole Mass Spectrometer with an Electrical Discharge Ion Source for Atmospheric Trace Gas Measurement. *Atmos. Meas. Tech.* **2019**, *12* (3), 1935–1954. https://doi.org/10.5194/amt-12-1935-2019.

(30) Haskins, J. D.; Jaeglé, L.; Shah, V.; Lee, B. H.; Lopez-Hilfiker, F. D.; Campuzano-Jost, P.; Schroder, J. C.; Day, D. A.; Guo, H.; Sullivan, A. P.; Weber, R.; Dibb, J.; Campos, T.; Jimenez, J. L.; Brown, S. S.; Thornton, J. A. Wintertime Gas-Particle Partitioning and Speciation of Inorganic Chlorine in the Lower Troposphere Over the Northeast United States and Coastal Ocean. *Journal of Geophysical Research: Atmospheres* **2018**, *123* (22), 12,812-897,916. https://doi.org/10.1029/2018JD028786.

(31) Angelucci, A. A.; Furlani, T. C.; Wang, X.; Jacob, D. J.; Vandenboer, T. C.; Young, C. J. Understanding Sources of Atmospheric Hydrogen Chloride in Coastal Spring and Continental Winter. *ACS Earth Space Chem* **2021**, *5* (9), 2507–2516. https://doi.org/10.1021/acsearthspacechem.1c00193.